

# Polar and non-polar atomic motions in the relaxor ferroelectric PLZT from dielectric, anelastic and NMR relaxation

F. Cordero<sup>1</sup>, M. Corti<sup>2</sup>, F. Craciun<sup>1</sup>, C. Galassi<sup>3</sup>, D. Piazza<sup>3</sup> and F. Tabak<sup>4</sup>

<sup>1</sup> CNR-ISC, Istituto dei Sistemi Complessi,

Area della Ricerca di Roma - Tor Vergata, Via del Fosso del Cavaliere 100, I-00133 Roma, Italy

<sup>2</sup> Dipartimento di Fisica "A. Volta" e unità INFN-CNR, Università di Pavia, Via Bassi 6, I-27100 Pavia, Italy

<sup>3</sup> CNR-ISTEC, Istituto di Scienza e Tecnologia della Ceramica, Via Granarolo 64, I-48018 Faenza, Italy

<sup>4</sup> Department of Physics Engineering, Hacettepe University, 06532 Beytepe, Ankara, Turkey

Dielectric, anelastic and <sup>139</sup>La NMR relaxation measurements have been made on the relaxor ferroelectric  $\text{Pb}_{1-3x/2}\text{La}_x\text{Zr}_{0.2}\text{Ti}_{0.8}\text{O}_3$  (PLZT) with  $x = 0.22$ . The dielectric susceptibility exhibits the frequency dispersive maximum due to the freezing of the polar degrees of freedom around  $T \simeq 250$  K. The anelastic and especially NMR relaxation, besides this maximum, indicate an intense and broad component at lower temperatures, attributed to rotational modes of the O octahedra, weakly coupled to the polar modes. It is discussed why such short range rotational instabilities, known to occur in the Zr-rich rhombohedral region of the PLZT phase diagram, might appear also in the Ti-rich region.

## I. INTRODUCTION

Much effort is being spent during the last years in trying to understand the so-called relaxor state of disordered ferroelectrics, and notably the perovskite relaxors, with general formula  $\text{ABO}_3$ . The technological interest arises from the fact that such materials may be prepared with very high values of dielectric, piezoelectric, electrostrictive and electro-optical constants in wide temperature ranges, finding applications like non-volatile and DRAM memories, capacitors, microelectromechanical devices, electro-optic modulators, optical switches etc.

Such materials have disorder in the cation sublattices that inhibits the formation of long range ferroelectric order,<sup>1</sup> and present a phenomenology similar to that found in spin glasses<sup>2</sup> and other glassy systems, with freezing of the polar fluctuations, separation of field cooled from zero field cooled susceptibility curves<sup>3</sup> and non equilibrium phenomena like aging and memory.<sup>4,5</sup> After the early explanation of the broadened maximum of the dielectric susceptibility in terms of a distribution of Curie temperatures, according to the local composition, other models have been proposed, *e.g.* in terms of quenched random fields due to compositional fluctuations,<sup>6</sup> and spin-glass state induced by interactions among the polar clusters<sup>2</sup> or random fields.<sup>7</sup> Recently, the spherical random-bond random-field model<sup>8</sup> has been developed, as a useful framework to understand several properties of the relaxor ferroelectrics.

Regarding the microscopic mechanism of the electric polarization, the focus has been on perovskites

having charge disorder in the B sublattice, like  $\text{Pb}(\text{Mg}_{1/3}\text{Nb}_{2/3})\text{O}_3$  (PMN). In these systems detailed studies of the atomic displacements have been carried out by neutron<sup>9,10</sup> and synchrotron x-ray<sup>11</sup> diffraction, and by x-ray absorption fine structure,<sup>12</sup> while the relevant phonon instabilities have been studied by inelastic neutron spectroscopy.<sup>13-15</sup> Much recent experimental<sup>16,17</sup> and theoretical<sup>18</sup> work is devoted even to the well known ferroelectric system  $\text{PbZr}_{1-y}\text{Ti}_y\text{O}_3$  (PZT) near the boundary at  $y \simeq 0.48$  between the Zr-rich rhombohedral and Ti-rich tetragonal phases.

Another perovskite relaxor system used in several applications is  $(\text{Pb}/\text{La})(\text{Zr}/\text{Ti})\text{O}_3$  (PLZT), obtained from PZT by substituting  $\text{Pb}^{2+}$  with  $\text{La}^{3+}$ . Since in this case the charge disorder is in the A sublattice, many of the considerations valid for B-disordered relaxors do not hold for PLZT. The most explored region of the PLZT phase diagram is the one around 65% of Zr, while only few studies are devoted to the Ti-rich one,<sup>19-21</sup> which show particularly high quadratic electro-optic effect and electrostrictive strain, useful for quadratic electro-optic modulators, optical phase retarders, electro-optical shutters and electrostrictive actuators.

In this report we present the results of a study of the atomic dynamics accompanying the freezing of polarization in La- and Ti-rich PLZT by measuring its dielectric susceptibility, elastic compliance and NMR relaxation rate of the <sup>139</sup>La nuclei. These experiments probe the fluctuations of the electric polarization, of strain and of the environment of the La nuclei, respectively.

## II. EXPERIMENTAL

Ceramic  $(\text{Pb}_{1-3x/2}\text{La}_x)(\text{Zr}_{0.2}\text{Ti}_{0.8})\text{O}_3$  (PLZT 100x/20/80), with the charge compensating vacancies in the Pb sublattice, has been prepared by using the mixed-oxide method according to the following processing route. The oxide powders were wet ball milled with zirconia balls in the stoichiometric amount for 24 h, the suspension was then freeze dried, sieved to 200  $\mu\text{m}$  and calcined at 850 °C for 4 hours. Samples of the calcined powders with  $x = 0, 2, 12, 22\%$  were pressed into bars and sintered at 1250 °C for 2 h, packed with  $\text{PbZrO}_3 + 5\text{wt}\%$  excess  $\text{ZrO}_2$  in order to maintain a constant PbO activity at the sintering temperature.

Phases and microstructure were investigated by x-ray diffraction (XRD) analysis and by SEM on fracture on a series of samples with  $0 \leq x \leq 0.22$ . For  $x = 0.22$ , the average grain size determined from SEM was  $3.2 \mu\text{m}$ , and the density was about 95% of the theoretical one. The XRD patterns in Fig. 1 show the presence of pure perovskitic phase with symmetry varying from tetragonal to pure cubic as the addition of La increases; the tetragonal distortion calculated over appropriate peaks of the diffractograms is shown in Fig. 2 to vary almost linearly from 5% for PZT 20/80 to  $< 0.2\%$  for PLZT 22/20/80. The composition under investigation here is PLZT 22/20/80, with a cubic cell and without long range ferroelectric order; in fact, ferroelectric hysteresis measurements showed a very slim loop with a remanent polarization of about  $1 \mu\text{C}/\text{cm}^2$  (typical values in the ferroelectric state are  $30 \mu\text{C}/\text{cm}^2$ ). Samples were cut as thin bars approximately  $45 \times 4 \times 0.5 \text{ mm}^3$ , the shape required by the anelastic spectroscopy experiments. After cutting, the samples were annealed for 15 h in air at  $750^\circ\text{C}$ ; the electrodes for the anelastic and dielectric spectroscopy measurements were applied with silver paint.

The dielectric susceptibility  $\chi = \chi' + i\chi''$  was measured with a HP 4194 A impedance bridge with a four wire probe and a signal level of  $0.5 \text{ V}/\text{mm}$ , between 200 Hz and 1 MHz. The measurements were made on cooling at  $1 - 1.5 \text{ K}/\text{min}$  from 570 to 200 K.

The complex Young's modulus  $E(\omega, T) = E' + iE''$  was measured on cooling by suspending the bar on thin thermocouple wires and electrostatically exciting its 1st and 5th flexural modes, whose resonance frequencies were  $\omega_i/2\pi \simeq 1.5$  and 20 kHz. The real part of the Young's modulus is related to the resonance frequency through  $\omega_i = \alpha_i \sqrt{E'/\rho}$ , where  $\alpha_i$  is a geometrical factor and  $\rho$  the mass density. The elastic energy loss coefficient, or the reciprocal of the mechanical quality factor,<sup>22</sup> is  $Q^{-1}(\omega, T) = E''/E' = s''/s'$ , where  $s = s' + is'' = E^{-1}$  is the elastic compliance; the  $Q^{-1}$  was measured from the decay of the free oscillations or from the width of the resonance peak. The elastic compliance  $s$  is the mechanical analogue of the dielectric susceptibility  $\chi$ .

The  $^{139}\text{La}$  NMR spectra and spin-lattice relaxation rates  $2W$  have been obtained by standard pulse techniques, operating in the quadrupole perturbed Zeeman regime, with external magnetic field  $H_0$  varying from 1.8 to 9 Tesla. The temperature range explored was 120–600 K. The spectra were obtained by the Fourier transform (FT) of the half of the echo signal and also by the envelope of the echo under sweeping the RF frequency. The echo signal arises from the powder distribution of the second-order quadrupole shift of the central line. From FT the central component showed a width of about 65 kHz. The satellite components are spread over a wide frequency range because of the first-order perturbation effects due to the electric quadrupole interaction. The pulse length maximizing the  $^{139}\text{La}$  quadrupolar echo signal was found about a factor 2 smaller than the pulse expected for La nuclei in the absence of quadrupole in-

teraction, indicating that the satellite lines are almost not irradiated. The relaxation time measurements were performed by monitoring the recovery of the echo amplitude after irradiation of the central line with a sequence of saturating pulses in a time much smaller than the recovery time. Even though the acquisition of the recovery of the nuclear magnetization lasted several hours, aging did not affect the measurements, since the aging effects decrease with increasing frequency. In order to assess the lack of influence from aging, the recovery of the nuclear magnetization was recorded using different sequences of delays and checking that the amplitude of the signals did not depend on the chosen sequence.

For the sake of illustration of the relationship between the different experimental techniques used in the present work, we anticipate here that in the ideal case that the main contribution to the nuclear relaxation process originates from the same type of atomic displacements  $u(t)$  that determine the dielectric and elastic uniform susceptibilities,  $2W$  could be qualitatively written in the form<sup>23</sup>

$$2W = A^2 \int \langle u(t) u(0) \rangle e^{-i\omega t} dt = A^2 J(\omega) \quad (1)$$

where  $A$  is a constant including the quadrupole moment of the  $^{139}\text{La}$  nucleus and the derivatives of the electric field gradient (EFG) components at the nuclear site with respect to the displacement  $u$ , while  $J(\omega)$  is the spectral density of the correlation function for  $u(t)$ . In this model situation, a simple relationship between the NMR relaxation rates and the dielectric data would be possible through the fluctuation-dissipation theorem,  $\chi''(\omega) \propto \frac{\omega}{T} J(\omega)$ . Later on we shall discuss the breakdown of such a direct connection.

### III. RESULTS

Figure 3 presents the real and imaginary parts of  $\chi(\omega, T)$  and  $s(\omega, T)$ , together with one of the  $\chi''_{\text{NMR}}(\omega, T)$  curves defined as  $\chi''_{\text{NMR}}(\omega, T) = \omega A^2 \frac{W}{k_B T}$  according to the aforementioned simplified model (for  $\omega = 2\pi \times 54 \text{ MHz}$ ). Even though all three types of relaxations present a maximum in correspondence with the relaxor transition around 250 K, there are substantial differences in the position and frequency dispersion of this peak, and in its low temperature tail. The comparison between dielectric susceptibility and elastic compliance is more direct, since both involve uniform susceptibilities  $\chi(q=0, \omega)$  in the same frequency ranges. The differences between the  $\chi$  and  $s$  curves indicate the presence of additional relaxation modes, besides the freezing of the polar degrees of freedom probed by  $\chi$ . For  $\chi''_{\text{NMR}}(\omega, T)$  one should take into account a sizeable contributions from dispersive relaxation modes at different wave vector which are not included in the uniform susceptibilities.

### A. Dielectric susceptibility

The  $\chi'(\omega, T)$  curves in Fig. 3 are in good agreement with the series of  $\chi'(\omega, T)$  curves for PLZT  $x/20/80$  with  $16 \leq x \leq 20$  already reported,<sup>21</sup> the maximum being slightly smaller and about  $\sim 50$  K lower in temperature with respect to the highest  $x$  reported there. In order to make a comparison with the NMR  $2W$  curves, we determine a fitting expression for  $\chi(\omega, T)$  that can be extrapolated at the NMR frequencies. The interpolation of the dielectric susceptibility involves the choice of a static susceptibility  $\chi(0, T)$ , and of a frequency dispersion function, generally taken as a superposition of elementary relaxation functions with a suitable distribution  $g(\ln \tau)$  of relaxation times, so that the dielectric susceptibility is expressed as

$$\chi(\omega, T) = \chi(0, T) \int d \ln \tau g(\ln \tau) \frac{1}{1 - i\omega\tau}. \quad (2)$$

In relaxor ferroelectrics,  $\chi(0, T)$  follows a modified Curie-Weiss law at temperatures sufficiently far from the relaxor peak, but there is no divergence on approaching it. For the present purposes, we limit ourselves to finding a phenomenological expression for  $\chi(0, T)$  that is suitable to fit the data down to temperatures as close as possible to the relaxor peak. An excellent fit can be obtained with a logistic function, which saturates at low  $T$  instead of diverging,

$$\chi(0, T) = \chi_0 + \frac{\Delta\chi}{1 + (T/T_0)^p} \quad (3)$$

with  $\chi_0 = 270$ ,  $\Delta\chi = 9260$ ,  $T_0 = 319$  K,  $p = 5.65$ . The value of  $\chi_0$  seems too high for representing the infinite frequency limit  $\chi_\infty$ , and is therefore considered as a fitting parameter in (3), while  $\chi_\infty$  is neglected; the fitting curve is shown in Fig. 4.

Regarding the frequency dispersion, we tried with exponential<sup>24</sup> and uniform<sup>25–27</sup> distribution functions in  $g(\ln \tau)$ . The first type of distribution function was adopted to interpret dielectric measurements on  $\text{Pb}(\text{Mg}_{1/3}\text{Nb}_{2/3})\text{O}_3$ ,<sup>24</sup> but could hardly reproduce the present data. Instead, we could interpolate reasonably well both  $\chi'$  and  $\chi''$  with a modified uniform distribution between  $\ln \tau_1$  and  $\ln \tau_2(T)$ , with the cutoff at the longest time broadened over  $w(T)$  in the logarithmic scale:

$$g(\ln \tau) = \begin{cases} g_0 \frac{1}{2} \left[ 1 - \tanh\left(\frac{\ln \tau - \ln \tau_2}{w}\right) \right] & \text{for } \tau > \tau_1 \\ 0 & \text{for } \tau < \tau_1 \end{cases} \quad (4)$$

$$g_0 = 2 / \left[ \ln \tau_2 / \tau_1 + w \ln \left[ 2 \cosh\left(\frac{\ln \tau_2 / \tau_1}{w}\right) \right] \right]$$

with  $w(T) = 0.15 \times (\ln \tau_2(T) - \ln \tau_1)$  scaling with the distribution width. The longest relaxation time at half maximum of the distribution has been assumed to follow the Vogel-Fulcher law, similarly to what observed for other compositions of PLZT<sup>3,27</sup>

$$\ln \tau_2 = \ln \tau_0 + E / (T - T_{\text{VF}}) \quad (5)$$

with  $\tau_0 = 10^{-14}$  s,  $E = 1450$  K and  $T_{\text{VF}} = 190$  K, while the fastest relaxation time has been set to  $\tau_1 = 5 \times 10^{-14}$  s. The  $\chi(\omega, T)$  curves have been obtained by numerically integrating eq. (2) and are shown in Fig. 5. The fit is optimized on  $\chi''(\omega, T)$  at the highest frequency, in order to obtain a reliable extrapolation of the spectral density

$$J(\omega, T) \propto \frac{T}{\omega} \chi''(\omega, T) \quad (6)$$

at the NMR frequencies. For  $w = 0$ ,  $\chi''$  has the analytical form  $\chi'' = \chi(0, T) (\ln \tau_2 / \tau_1)^{-1} [\arctan(\omega\tau_2) - \arctan(\omega\tau_1)]$ , which is valid also for  $w \neq 0$  and  $T$  below the maximum, where the shape of the cutoff at  $\omega\tau_2 \gg 1$  has no influence. The low  $T$  approximation is therefore  $\chi''(\omega, T) \simeq \chi(0, T) \frac{\pi}{2} \left( \frac{T - T_{\text{VF}}}{E_2 - E_1} \right)$ , where the linear increase with  $T$  above  $T_{\text{VF}}$  comes from the  $T$  dependent normalization factor  $(\ln \tau_2 / \tau_1)^{-1}$ ; therefore, considering the weak temperature dependence of  $\chi(0, T)$  below the maximum,  $T_{\text{VF}}$  is the temperature at which the linear extrapolation of  $\chi''$  below the maximum vanishes. Of course, there is no real divergence of the distribution width and the dielectric susceptibility does not vanish below  $T_{\text{VF}}$ , but the Vogel-Fulcher hypothesis allows the dispersive maximum to be well described.

### B. Elastic compliance

The elastic compliance curves  $s(\omega, T)$  measured at the 1st and 5th resonance frequencies (1.5 and 20 kHz) are shown in Fig. 3 together with the susceptibility curves. The curves are normalized to the extrapolated value of  $s'$  at infinite temperature,  $s_\infty$ , which should be the equivalent of  $\chi_\infty$ . An important difference between the dielectric and the elastic susceptibilities, however, is that in relaxor ferroelectrics  $\chi_\infty$  brings a negligible contribution to the dielectric response; in fact,  $\chi_\infty$  is expected<sup>28</sup> to be  $\lesssim 10$  (even though  $\chi_\infty \sim 200$  has been reported in PLZT 9/65/35<sup>29</sup>) and here it is  $\chi' \sim 7000$  at the maximum. Instead, the background lattice contribution to  $s'$  is much more important: the peak value of  $s'$  is only 1.6 times larger than  $s_\infty$ . Since the lattice contribution to  $s'$  is also temperature dependent, it is easier to compare only the imaginary parts of the different susceptibilities, to which  $s_\infty$  and  $\chi_\infty$  do not contribute. The elastic  $s(\omega, T)$  differs from  $\chi(\omega, T)$  in three ways: *i*) the maxima of the real and imaginary parts are at lower temperature; *ii*) the frequency dispersion is smaller both in temperature shift and change of intensity, and the amplitude dependence of  $s'$  is reversed with respect to  $\chi'$ ; *iii*) the low temperature tail is much higher than in the dielectric case ( $s''(150 \text{ K})/s''(T_{\text{max}}) = 0.5$  for the elastic case at 20 kHz, while  $\chi''(150 \text{ K})/\chi''(T_{\text{max}}) = 0.07$  at 10 kHz). The comparison between  $\chi''$  and  $s''$  is rather

straightforward, since they both represent uniform susceptibilities. The only differences are in the relaxation strengths, which are sensitive to changes in electric dipolar degrees of freedom in one case and elastic quadrupolar in the other. In the simplest case of independent relaxing units, e.g. off-centre atoms hopping between positions  $i$  and  $j$  with a correlation time  $\tau$  one has<sup>22</sup>

$$\Delta\chi(0, T) = \frac{(\Delta p)^2}{k_B T}, \quad \Delta s(0, T) = \frac{(\Delta\lambda)^2}{k_B T} \quad (7)$$

where  $\Delta\mathbf{p} = \mathbf{p}^{(i)} - \mathbf{p}^{(j)}$  is the change of the electric dipole during the jump, and  $\Delta\lambda = \lambda^{(i)} - \lambda^{(j)}$  is the change of the elastic quadrupole (generally called elastic dipole<sup>22</sup> for analogy with the electric and magnetic cases). The relaxation of a same unit may produce a change in  $\mathbf{p}$  but not in  $\lambda$ , e.g. the reorientation of an off-centre unit by  $180^\circ$  changes  $\mathbf{p}$  to  $-\mathbf{p}$  but does not affect  $\lambda$ , which is a centrosymmetric strain (representable as a strain ellipsoid). Conversely, there may be relaxation modes affecting  $\lambda$  but not  $\mathbf{p}$ , e.g. rotations or distortions of the octahedra. The differences in the dielectric and elastic susceptibilities indicate that the latter is little affected by the dipolar relaxation, since the peak in  $s''$  is not proportional to the relaxor peak in  $\chi''$ ; in addition, there are other relaxation modes almost invisible to  $\chi$ , but contributing to  $s$  below the relaxor transition. These modes are faster and only loosely follow the dipolar freezing, as indicated by the lower temperature of the peak and the huge low temperature tail.

The role of electrostrictive strain in driving the anelastic relaxation in relaxor ferroelectrics has been emphasized,<sup>21,30</sup> but cannot account for the present results; in fact, if the strain fluctuations were simply driven by the dipolar ones through electrostriction,  $s''$  would follow  $\chi''$  much more closely, since the electrostrictive coupling is expected to be weakly dependent on temperature.

### C. NMR

Under the conditions of measurements outlined in Section II, by solving the master equations for  $I = 7/2$ , the recovery of the echo signal is expected to be described by the law

$$y(t) = 0.012 e^{-0.47Wt} + 0.714 e^{-1.33Wt} + 0.068 e^{-2.4Wt} + 0.206 e^{-3.8Wt} \quad (8)$$

In deriving Eq. (8) the relaxation transition probability  $W_1$  and  $W_2$  ( $\Delta m = 1$  and  $\Delta m = 2$  transitions respectively) have been assumed practically equal, as usual in powdered samples.<sup>23</sup> At high temperatures, well above the ferroelectric relaxor transition temperature, the recovery of the echo signal is rather well fitted by Eq. (8), as shown by the solid line in Fig. 6. One notes that, according to Eq. (8), the relaxation rate  $2W$  can also be

obtained from the time  $t^*$  where  $y(t^*) = 0.41$ , yielding  $2W = (t^*)^{-1}$ .

In the low temperature range Eq. (8) does no longer describe the recovery of the echo (see Fig. 6). This is the obvious consequence of the fact that, on approaching the relaxor transition temperature, each exponential in Eq. (8) becomes stretched. A meaningful fitting according to Eq. (8) is hardly possible, and thus in the low temperature range ( $T < 300$  K) an effective  $2W$  has been extracted as the inverse of the time  $t^*$ .

The <sup>139</sup>La relaxation rates  $2W$  are reported in Fig. 7 for three representative measuring frequencies  $\omega/2\pi$ . From 700 K,  $2W$  increases on decreasing temperature passing through a maximum and then decreasing again. The maxima in  $2W$  occur in the temperature range where the maxima in imaginary part of the dielectric constant are also detected (see Fig. 3). This suggests that, at least in the high temperature range, the mechanisms responsible of the reorientations of the electric dipole moments are also involved in the <sup>139</sup>La relaxation process. It should be remarked that, by varying the magnetic field from  $H_0 = 1.8$  T to  $H_0 = 9$  T, the maxima of  $2W$  do not sizably shift in temperature. This direct qualitative observation by itself suggests that the freezing process involves a large distribution of correlation times, as can be expected for a strongly disordered relaxor.

In the weak collision approach, for overdamped phonon modes and/or localized modes in disordered systems (direct relaxation process) the relaxation rate driven by the time dependence of the EFG components can be written in the form anticipated in Eq. (1), where the spectral density  $J_1(\omega)$  and  $J_2(2\omega)$  have been assumed practically coincident. We can explicitate the constant  $A^2$  and write  $2W$  in the form  $2W \simeq 5\langle\omega_Q^2\rangle_{fl} J(\omega)$ ,  $\langle\omega_Q^2\rangle_{fl}$  being an average effective strength of the time dependent quadrupole coupling and  $J(\omega)$  the spectral density of the reduced correlation function.<sup>23</sup> For monodisperse processes, with a single correlation time, the spectral density would be  $J(\omega) = 2\tau/(1 + \omega^2\tau^2)$ . In the fast motions regime, i.e.  $\tau^{-1} \gg \omega$ , one would have a frequency independent  $2W$  of the order of  $2W \simeq 12\langle\omega_Q^2\rangle_{fl}\tau$ , while for slow motions ( $\tau^{-1} \ll \omega$ ) it is  $2W \simeq 10\langle\omega_Q^2\rangle_{fl}(\omega^2\tau)^{-1}$ . From the value of  $2W$  at the maximum an order of magnitude of the fluctuating quadrupole coupling constant can be derived:  $\langle\omega_Q^2\rangle_{fl}^{1/2} \simeq (2W_m/\omega)^{1/2} \simeq 50 - 100$  kHz, a reasonable value for the motions around the equilibrium position of the ions. In the present case, the  $\omega$  dependence of  $2W$  is reduced by the broad distribution of correlation times typical of relaxors. We first tried with the same uniform distribution function adopted for the dielectric case, but it is apparent from Fig. 8 that the extrapolation of the  $(T/\omega)\chi''(\omega, T)$  curves to the NMR frequencies does not properly reproduce  $2W$ . We therefore tried with the distribution proposed by Lu and Calvarin<sup>24</sup> (LC) for their dielectric relaxation data in  $\text{Pb}(\text{Mg}_{1/3}\text{Nb}_{2/3})\text{O}_3$  and  $\text{Pb}_2\text{KTa}_5\text{O}_{15}$ . The LC distribution is assumed in the form

$$P(E) = \begin{cases} w^{-1}e^{(E_C-E)/w} & \text{for } E \geq E_C \\ 0 & \text{for } E < E_C \end{cases} \quad (9)$$

where  $E = KV$  is the activation energy for thermal fluctuations of a polar cluster in the paraelectric matrix, proportional to its volume.  $E_C = KV_C$  is the minimum activation energy corresponding to a critical volume of the order of the volume of a crystalline cell. The temperature dependence of the distribution width  $w$  has been assumed of the form  $w = E_0 e^{E_1/T}$ . The correlation times are related to the activation energies by  $\tau = \tau_0 e^{E/T}$ . In Fig. 7 the lines represent the temperature dependence of  $2W$  numerically obtained in the assumption of LC distribution with  $\tau_0 = 10^{-13}$  s,  $E_C = 100$  K,  $E_0 = 115$  K and  $E_1 = 750$  K. The fit of the experimental results, although better than the simple extrapolation of the dielectric ones, is again poor.

A detailed series of measurements as a function of  $\omega$  has been carried out at constant temperature,  $T = 140$  K, below the maxima in  $2W$  vs  $T$ . In Fig. 9 the experimental data at  $T = 140$  K have been compared with the frequency dependence expected on the basis of the relaxation rates according to the LC distribution (dashed line) and to a uniform distribution (dotted line). It is evident that both the absolute values as well as the frequency dependence do not agree with the theoretical expectations according to the above models. Here we note that a good fit could be obtained if a frequency independent contribution, arising from a second type of motion effective in the relaxation process, is added to the frequency behavior of the LC distribution (solid line). As noted above, an almost frequency independent contribution implies a prevalence of fast motions, with  $\omega\tau \ll 1$  still at 140 K, consistent with the broad contribution at low temperature both in  $2W$  and in the anelastic  $s''$ . We conclude that the  $^{139}\text{La}$  NMR relaxation contains additional contributions with respect to the dipolar freezing dominating the dielectric susceptibility, especially in the low temperature region.

## IV. DISCUSSION

### A. Non-polar relaxation modes

The comparison between dielectric, anelastic and NMR relaxations indicates the existence of at least two distinct types of atomic motions: *i*) polar modes that dominate the behavior of  $\chi''$ , giving rise to the typical relaxor maximum, but are less evident in  $s''$  and  $2W$ ; *ii*) other modes, affecting much less  $\chi$  and dominating the nuclear magnetic and anelastic relaxations. The second type of modes prevails at lower temperature and should be essentially non-polar, since it does not appear in the dielectric relaxation.

A comparison between dielectric and anelastic relaxation in PLZT 9/65/35, shows even larger differences,<sup>31</sup> since  $s''$  completely lacks the relaxor peak and only

presents a step-like increase at a temperature  $\sim 30$  K lower than that of the relaxor peak in  $\chi''$ ; this is shown in Fig. 10. It was proposed that the main difference between the two types of responses consists in the lack of sensitivity of the elastic compliance to the  $180^\circ$  switching of the polarization, which would be the main responsible for the relaxor peak; the non- $180^\circ$  polarization dynamics, contributing also to  $s''$ , would instead have an increasing role at lower temperature.<sup>31</sup> The NMR data, however, suggest a different picture; in fact, there is no reason to suppose that the  $^{139}\text{La}$  nuclear relaxation should be much more sensitive to non- $180^\circ$  rather than to  $180^\circ$  polarization dynamics, and therefore the explanation of the predominant weight of relaxation in  $2W$  at temperature lower than that of the relaxor peak can hardly rely on non- $180^\circ$  polarization dynamics. Rather, this indicates that the NMR relaxation probes a non-polar dynamics, not appearing in  $\chi$ , presumably the same type of motion appearing in the anelastic response. Motions of this type may be rotations or distortions of the octahedra and antiferrodistortive displacements of the cations.

### B. Rotations of the octahedra

Rotations or deformations of the octahedra would certainly provide a strong contribution to  $2W$ , since a La ion is surrounded by 12 nearest neighbor O atoms at  $a/\sqrt{2}$ , and 8 second neighbor Ti/Zr atoms at  $\sqrt{3}/2 a$ ; the contribution of the atomic shifts to the EFG fluctuations decreases with the 6th power of the distance from the La site, so that the contribution from motions of the O octahedra (or of La with respect to the surrounding octahedra) is enhanced by 5 times over the contribution from the motion of the Zr/Ti atoms. Since the microscopic polarization in PLZT is mainly attributed to the off-centre displacements of the cations with respect to the O octahedra, and there is little correlation between these polar fluctuations and  $2W$ , it seems reasonable to assign the main contribution to the NMR relaxation to rotations or deformations of the octahedra.

Distortions of the octahedra of the Jahn-Teller type are found in perovskites with cations supporting mixed valence, like manganites, but this is not the case of ferroelectric PLZT, where both Zr and Ti have fixed valence +4. Jahn-Teller polarons in ferroelectric perovskites may be observed only after suitable doping,<sup>32</sup> e.g. in Nb-doped  $\text{BaTiO}_3$  where each  $\text{Nb}^{5+}$  is compensated by one Jahn-Teller active  $\text{Ti}^{3+}$ ; our samples might well contain some minority charged defects, like O vacancies, but they are insulators and a mechanism like a Jahn-Teller polaron cannot be considered as source of the intense relaxation observed below the relaxor transition.

Rotations of the octahedra are instead typical of all perovskites, including the ferroelectric ones, and the low temperature phases of Zr-rich PZT are the result of the condensation of unstable rotational modes of the O octa-

hedra, together with ferro- and antiferroelectric modes of the cation sublattices.<sup>33,34</sup> The PZT phase diagram<sup>16,35</sup> grossly consists of a cubic high temperature phase, which transforms into ferroelectric tetragonal for a Ti fraction  $y > 0.48$  and ferroelectric rhombohedral below the almost temperature independent boundary  $y \simeq 0.48$ . In the tetragonal phase, the A (Pb) and B (Zr/Ti) sublattices are shifted along the  $c$  axis with respect to the O octahedra, which are additionally elongated. This is seen as the result of the condensation of the unstable  $\Gamma_{15}$  phonon. In the rhombohedral phase the cations are shifted along the pseudocubic [111] direction, and, below a certain temperature, the octahedra rotate about the polar [111] axis, giving rise to the low-temperature rhombohedral phase. Additional rotational instabilities of local character have been proposed to exist in Zr-rich PZT<sup>36</sup> and especially in PLZT.<sup>35,37</sup> Viehland and coworkers found  $\frac{1}{2}\langle 111 \rangle$  and  $\frac{1}{2}\langle 110 \rangle$  superlattice spots in electron diffraction by TEM, which they associate with coordinated rotations of the octahedra by an angle  $\pm\phi$  about the pseudocubic  $c$  axis, with successive layers in phase (condensation of the  $M_3$  phonon mode<sup>38</sup> producing  $\frac{1}{2}\langle 110 \rangle$  reflections) or antiphase ( $R_{25}$  mode producing  $\frac{1}{2}\langle 111 \rangle$  reflections). These reflections progressively disappear with increasing Ti content, and in PLZT 12/40/60 only weak spots were found in a minority fraction of the selected areas.<sup>37</sup> It has later been argued<sup>16</sup> that such superlattice reflections might mainly arise from additional shifts of the Pb atoms along pseudocubic [100] directions, coupled with the octahedral rotations; in addition, since these reflections are not observed by x-ray or neutron diffraction, the regions of additional  $M_3$  or  $R_{25}$  ordered rotations might exist only near the surface of grains, at least in La-free PZT. Rotational instabilities of  $M_3$  and  $R_{25}$  type have also been found in first-principle calculations of the phonon instabilities in rhombohedral PZT.<sup>34</sup>

While the existence of these rotational instabilities is well documented in the rhombohedral region of the phase diagram of PZT and PLZT, we are not aware of any such observation in Ti-rich PLZT. Therefore, octahedral rotations seem at first unlikely to occur in our PLZT 22/20/80, considering that the parent PZT 20/80 is well within the tetragonal region of the phase diagram. We argue, however, that the substitution of Pb with La changes the situation considerably with respect to PZT. First of all, XRD measurements on a series of samples with increasing La content (Fig. 1) show that the addition of La suppresses the tetragonal distortion, which is 5% in PZT 2/20/80, 2% in PLZT 12/20/80, and  $< 0.2\%$  in PLZT 22/20/80, implying the absence of a strong stabilization of the tetragonal phase in the present case. A similar behavior has been found in PLZT  $x/40/60$ .<sup>20</sup> The La addition should also favor the rotational instability at the expenses of the tetragonal one. In fact, calculations of the phonon dispersions<sup>28,33</sup> show that both the  $\Gamma_{15}$  tetragonal and the rotational  $R_{25}$  instabilities exist in

PbTiO<sub>3</sub> and PbZrO<sub>3</sub>, although the  $\Gamma_{15}$ , mainly consisting in a displacement of Pb along (001),<sup>39</sup> is stabilized in PbTiO<sub>3</sub> by the tendency of Pb to shift in that direction in order to hybridize and form 4 short Pb-O bonds; this is possible, since also the Ti ions shift off-centre from the octahedra in the same direction, away from the O atoms with short Pb-O bonds. In PbZrO<sub>3</sub> instead, where the ideal Zr-O bonds are longer than the Ti-O ones, the rotational instability prevails in order to accommodate the larger octahedra; this fact is usually expressed in terms of the tolerance factor<sup>40</sup>  $t = (r_A + r_O) / \sqrt{2}(r_B + r_O)$  which is 1 if the ideal B-O distance matches the ideal A-O distance, and is  $< 1$  when the octahedra are too large to fit the cell and tend to rotate to maintain their size. The substitution of Pb with La should favor the rotational instability because: *i*) it decreases the tolerance factor, due to a smaller ideal La<sup>3+</sup>-O bond length (2.76 Å) with respect to Pb<sup>2+</sup>-O (2.89 Å),<sup>41</sup> and in fact XRD showed that the cell volume passed from 65 Å<sup>3</sup> in PZT 20/80 to 63.4 Å<sup>3</sup> in PLZT 22/20/80 (Fig. 2); *ii*) La<sup>3+</sup> does not have the ability of stabilizing the ferroelectric tetragonal mode by a large electronic hybridization with O, as Pb does.<sup>18,41</sup>

We think that the best candidates for the non-polar motions we observe are rotations of the octahedra related to the antiferrodistortive  $R_{25}$  mode described above. First-principle calculations of the phonon dispersions showed that such a mode is unstable also in PbTiO<sub>3</sub>, although not enough to produce the ground state.<sup>28</sup> The dispersion curves indicate a strong correlation of the cooperative rotations about  $c$  within the  $ab$  plane, due to the corner sharing of the octahedra, but little correlation along  $c$  (the same mode, with full correlation also along  $c$ , is responsible for the cubic to tetragonal transformation in SrTiO<sub>3</sub><sup>42</sup>). Due to the lack of correlation between different planes even in pure PbTiO<sub>3</sub> and to the strong disorder in the A sublattice in PLZT 22/20/80, the local condensation of such a mode over only few octahedra should be possible, without producing superlattice peaks in diffraction patterns. In addition, the small correlation length and frustration from disorder would make it possible to switch between differently rotated configurations. Switching between rotated and non-rotated configurations would be accompanied by a change of the in-plane shear strain (corresponding to  $\Delta\lambda \neq 0$  in Eq. (7)) and therefore by anelastic relaxation, while the NMR relaxation would be sensitive also to switching between correlated rotations by opposite angles (which leave strain unchanged) and to the anharmonic dynamics related to such an unstable mode.

Finally, the rotations of the octahedra are only weakly coupled to the cation displacements in PLZT,<sup>43</sup> the major coupling perhaps coming from the tendency of Pb to form four short Pb-O bonds.<sup>16</sup> In fact, recent powder neutron diffraction experiments on rhombohedral PZT have been interpreted assuming that, besides the established ferroelectric displacements of Pb along the pseudocubic (111) direction, additional (100) shifts of  $\sim 0.2$  Å

are induced by the tendency of Pb to form the fourfold coordination with the surrounding O atoms, with the choice between  $x$ ,  $y$  or  $z$  dictated by the local tilt pattern of the octahedra.<sup>16</sup> Then, the weak coupling between the ferroelectric cation displacements and the octahedra rotations justify the fact that the latter are still fast at temperatures at which the polar modes are completely frozen out; on the other hand, the weak low temperature tail found also in the dielectric  $\chi''$  might result from the supposed additional degree of freedom of Pb,<sup>16</sup> which is coupled to the octahedra (besides the fact that disorder might induce a polar component also to the rotations of the octahedra).

Further support to the hypothesis that rotations of the octahedra are responsible for the low temperature NMR and anelastic relaxation comes from the comparison of the anelastic spectra of PLZT 22/20/80 and PLZT 9/65/35,<sup>31</sup> shown in Fig. 10. The latter composition is in the rhombohedral region of the phase diagram, where the rotational instabilities are documented, and in fact the low temperature component alone determines the anelastic spectrum of PLZT 9/65/35, whereas it is less important in PLZT 22/20/80.

### C. Antiparallel cation motion

In principle, also correlated antiparallel motions of the A or B cations might explain the discrepancies between the dielectric relaxation on one side and the NMR and anelastic relaxation on the other side, since they produce fluctuations both in shear strain and on the EFG at the La site, but negligible dielectric response. Such modes are responsible for the antiferroelectric phases in the Zr-rich end of the PLZT phase diagram, but we do not see reasons why they should have importance in PLZT with 80% of Ti. In addition, such antiferroelectric modes involve displacements of the Pb atoms;<sup>44</sup> therefore, their condensation should be hindered by the strong disorder in the A sublattice, and, if it occurred, it would result in a polar mode, due to the charge variations among different A sites (Pb<sup>2+</sup>, La<sup>3+</sup> and vacancies). We conclude that the extra contribution to the relaxation process found in the anelastic and NMR experiments is rather due to modes involving the O octahedra.

## V. CONCLUSION

The combination of dielectric, NMR and anelastic spectroscopies in the relaxor ferroelectric PLZT reveals that, besides the polar fluctuations freezing at the relaxor transition, other fluctuations of the atomic positions exist, that are faster and weakly correlated with the polar ones. In fact, the imaginary dielectric susceptibility  $\chi''(\omega, T)$  presents the usual peak, with a frequency dispersion signaling the freezing of the polar degrees of

freedom, and a weak tail at lower temperature, while the curves of the imaginary elastic compliance  $s''(\omega, T)$  and especially of the <sup>139</sup>La NMR relaxation rate  $2W$  versus temperature present a more intense component at lower temperatures. This low temperature relaxation has been assigned to non polar modes, which have been argued to correspond to rotations of the octahedra; in particular, on the basis of the calculated phonon dispersion curves in the PZT system,<sup>28,33</sup> it is suggested that the condensation of the  $R_{25}$  mode might lead to clusters of rotated octahedra about the pseudocubic  $c$  axis. The correlation lengths for such correlated rotations should be very short, due to the high concentration of La<sup>3+</sup> and Pb vacancies, which hinder the otherwise predominant ferroelectric tetragonal distortion. The small correlation length and the weak coupling with the other ferroelectric modes would make it possible for such clusters of octahedra to switch between differently rotated configurations, giving rise to the observed low temperature relaxation.

## VI. ACKNOWLEDGMENTS

The authors thank A. Rigamonti for useful discussions and for his advices. Thanks are also due to E.R. Mognaschi for his careful check of the dielectric measurements and for useful discussions.

## VII. FIGURE CAPTIONS

FIG. 1. Diffractograms of PLZT x/20/80 at four La contents.

FIG. 2. Vanishing of the tetragonal distortion with increasing La content.

FIG. 3. Real (upper panel) and imaginary parts (lower panel) of the dielectric susceptibility  $\chi$  (right ordinates) and elastic compliance  $s$  (left ordinates), measured at the frequencies indicated in the figure. Also shown is  $\chi''_{\text{NMR}}$  defined in the text measured at 54 MHz.

FIG. 4. Real part of the dielectric susceptibility measured at various frequencies. The thick line is  $\chi'(0, T)$  adopted for fitting  $\chi(\omega, T)$ .

FIG. 5. Real and imaginary parts of the experimental dielectric susceptibility (thick lines) and fitting curves (thin lines).

FIG. 6. Recovery behavior of the NMR echo signal after a RF pulse sequence saturating the central ( $+1/2 \leftrightarrow -1/2$ ) transition for different temperatures (squares 600 K, diamonds 179 K and stars 120 K). At high temperature the recovery is well described by Eq. (8) (solid line). In the low temperature range the recovery shows the change over to stretched exponentials.

FIG. 7. Temperature dependence of the NMR relaxation rates  $2W$  for different measuring frequencies. The lines represent the theoretical curves assuming the LC distribution (see text).

FIG. 8. Comparison between the NMR relaxation rates  $2W$  and the  $J(\omega, T)$  curves extrapolated from the fits to  $\chi''(\omega, T)$  of Fig. 5.

FIG. 9.  $2W$  relaxation rates at  $T = 140$  K as a function of the measuring frequency (filled squares). The lines give the frequency dependence expected for the uniform distribution of the correlation time (dashed line) and for the LC model (dotted-dashed line). The solid line is obtained by adding to the LC behavior a frequency independent contribution of  $0.29 \text{ ms}^{-1}$ .

FIG. 10. Comparison between the imaginary parts of the dielectric susceptibilities (upper panel) and elastic compliances (lower panel) of PLZT 9/65/35 and PLZT 22/20/80.

---

<sup>1</sup> L.E. Cross, *Ferroelectrics* **76**, 241 (1987).  
<sup>2</sup> D. Viehland, S.J. Jang, L.E. Cross and M. Wuttig, *J. Appl. Phys.* **68**, 2916 (1990).  
<sup>3</sup> Z. Kutnjak, C. Filipič, R. Pirc, A. Levstik, R. Farhi and M. El Marssi, *Phys. Rev. B* **59**, 294 (1999).  
<sup>4</sup> E.V. Colla, L.K. Chao, M.B. Weissman and D.D. Viehland, *Phys. Rev. Lett.* **85**, 3033 (2000).  
<sup>5</sup> F. Cordero, F. Craciun, A. Franco, D. Piazza and C. Galassi, *Phys. Rev. Lett.* **93**, 97601 (2004).  
<sup>6</sup> V. Westphal, W. Kleemann and M.D. Glinchuk, *Phys. Rev. Lett.* **68**, 847 (1992).  
<sup>7</sup> B.E. Vugmeister and H. Rabitz, *Phys. Rev. B* **57**, 7581 (1998).  
<sup>8</sup> R. Pirc and R. Blinc, *Phys. Rev. B* **60**, 13470 (1999).  
<sup>9</sup> B. Dkhil, J.M. Kiat, G. Calvarin, G. Baldinozzi, S.B. Vakhrušev and E. Suard, *Phys. Rev. B* **65**, 24104 (2002).  
<sup>10</sup> P. Juhas, I. Grinberg, A.M. Rappe, W. Dmowski, T. Egami and P.K. Davies, *Phys. Rev. B* **69**, 214101 (2004).  
<sup>11</sup> D.M. Fanning, I.K. Robinson, S.T. Jung, E.V. Colla, D.D. Viehland and D.A. Payne, *J. Appl. Phys.* **87**, 840 (2000).  
<sup>12</sup> A.I. Frenkel, D.M. Pease, J. Giniewicz, E.A. Stern, D.L.

Brewe, M. Daniel and J. Budnick, *Phys. Rev. B* **70**, 14106 (2004).  
<sup>13</sup> P.M. Gehring, S. Wakimoto, Z.-G. Ye and G. Shirane, *Phys. Rev. Lett.* **87**, 277601 (2001).  
<sup>14</sup> S.B. Vakhrušev and S.M. Shapiro, *Phys. Rev. B* **66**, 214101 (2002).  
<sup>15</sup> S. Wakimoto, C. Stock, Z.-G. Ye, W. Chen, P.M. Gehring and G. Shirane, *Phys. Rev. B* **66**, 224102 (2002).  
<sup>16</sup> D.L. Corker, A.M. Glazer, R.W. Whatmore, A. Stallard and F. Fauth, *J. Phys.: Condens. Matter* **10**, 6251 (1998).  
<sup>17</sup> R. Guo, L.E. Cross, S-E. Park, B. Noheda, D.E. Cox and G. Shirane, *Phys. Rev. Lett.* **84**, 5423 (2000).  
<sup>18</sup> I. Grinberg, V.R. Cooper and A.M. Rappe, *Nature* **419**, 909 (2002).  
<sup>19</sup> X. Dai, A. DiGiovanni and D. Viehland, *J. Appl. Phys.* **74**, 3399 (1993).  
<sup>20</sup> X.H. Dai, Z. Xu and D. Viehland, *Phil. Mag. B* **70**, 33-48 (1994).  
<sup>21</sup> X. Dai, Z. Xu and D. Viehland, *J. Appl. Phys.* **79**, 1021 (1996).  
<sup>22</sup> A.S. Nowick and B.S. Berry, *Anelastic Relaxation in Crystalline Solids*. (Academic Press, New York, 1972).  
<sup>23</sup> A. Rigamonti, *Advan. Phys.* **33**, 115 (1984).  
<sup>24</sup> Z.G. Lu and G. Calvarin, *Phys. Rev. B* **51**, 2694 (1995).  
<sup>25</sup> E.R. Mognaschi, A. Rigamonti and L. Menafrà, *Phys. Rev. B* **14**, 2005 (1976).  
<sup>26</sup> S.N. Dorogovtsev and N.K. Yushin, *Ferroelectrics* **112**, 27 (1990).  
<sup>27</sup> S. Kamba, V. Bovtun, J. Petzelt, I. Rychetsky, R. Mizaras, A. Brilingas, J. Banys, J. Grigas and M. Kosec, *J. Phys.: Condens. Matter* **12**, 497 (2000).  
<sup>28</sup> Ph. Ghosez, E. Cockayne, U.V. Waghmare and K.M. Rabe, *Phys. Rev. B* **60**, 836 (1999).  
<sup>29</sup> V. Bobnar, Z. Kutnjak, R. Pirc, R. Blinc and A. Levstik, *Phys. Rev. Lett.* **84**, 5892 (2000).  
<sup>30</sup> D. Viehland, S.J. Jang, E. Cross and M. Wuttig, *J. Appl. Phys.* **69**, 6595 (1991).  
<sup>31</sup> F. Cordero, F. Craciun, A. Franco and C. Galassi, *Ferroelectrics* **302**, 467 (2004).  
<sup>32</sup> S. Lenjer, O.F. Schirmer, H. Hesse and Th.W. Kool, *Phys. Rev. B* **66**, 165106 (2002).  
<sup>33</sup> M. Fornari and D.J. Singh, *Phys. Rev. B* **63**, 92101 (2001).  
<sup>34</sup> K. Leung, *Phys. Rev. B* **67**, 104108 (2003).  
<sup>35</sup> X. Dai, Z. Xu and D. Viehland, *J. Am. Ceram. Soc.* **78**, 2815 (1995).  
<sup>36</sup> D. Viehland, *Phys. Rev. B* **52**, 778 (1995).  
<sup>37</sup> D. Viehland, Z. Xu and D.A. Payne, *J. Appl. Phys.* **74**, 7454 (1993).  
<sup>38</sup> Y. Fujii, S. Hoshino, Y. Yamada and G. Shirane, *Phys. Rev. B* **9**, 4549 (1974).  
<sup>39</sup> U.V. Waghmare and K.M. Rabe, *Phys. Rev. B* **55**, 6161 (1997).  
<sup>40</sup> S.V. Halilov, M. Fornari and D.J. Singh, *Phys. Rev. B* **69**, 174107 (2004).  
<sup>41</sup> S. Teslic, T. Egami and D. Viehland, *J. Phys. Chem. Sol.* **57**, 1537 (1996).  
<sup>42</sup> J.F. Scott, *Rev. Mod. Phys.* **46**, 83-128 (1974).  
<sup>43</sup> N. Cereceda, B. Noheda, T. Iglesias, J.R. Fernandez - del Castillo, J.A. Gonzalo, N. Duan, Y.L. Wang, D.E. Cox and G. Shirane, *Phys. Rev. B* **55**, 6174 (1997).



<sup>44</sup> S. Watanabe and Y. Koyama, Phys. Rev. B **63**, 134103 (2001).

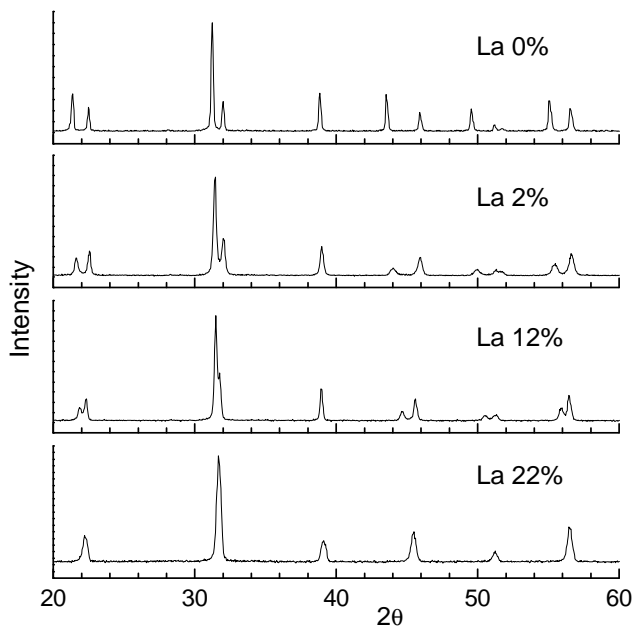


Fig. 1

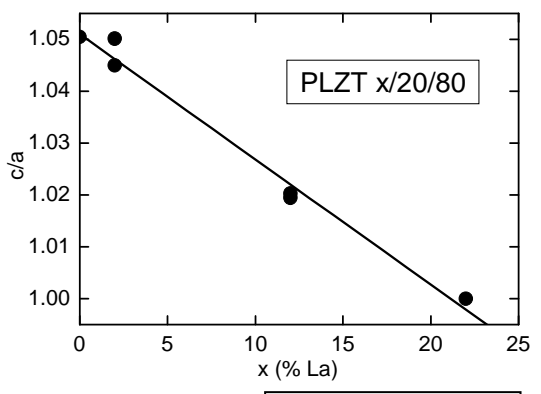


Fig. 2

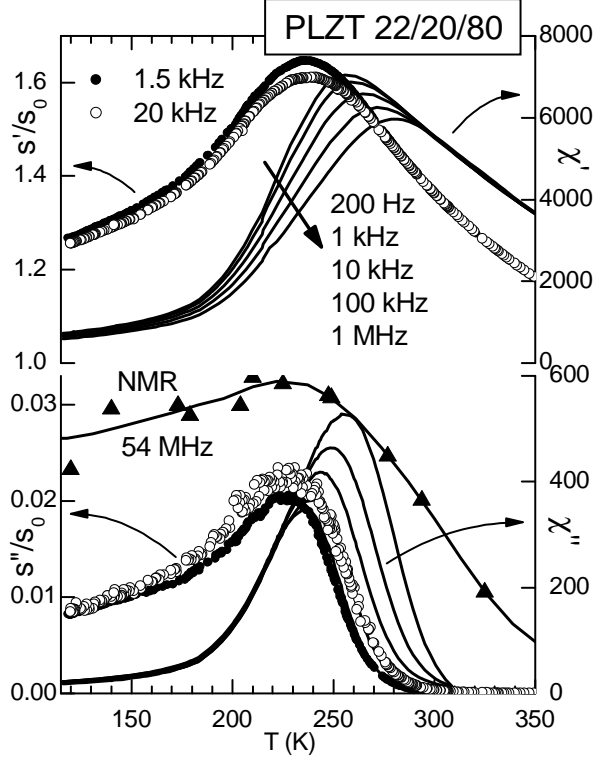


Fig. 3

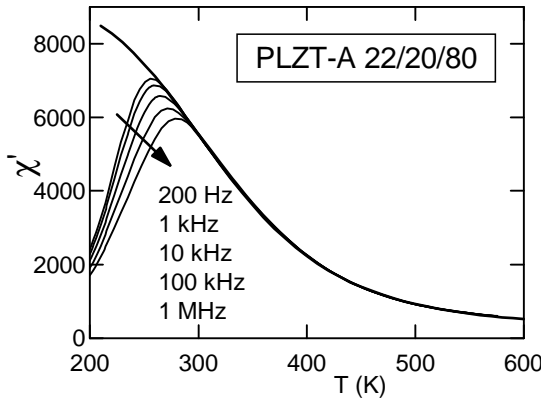


Fig. 4

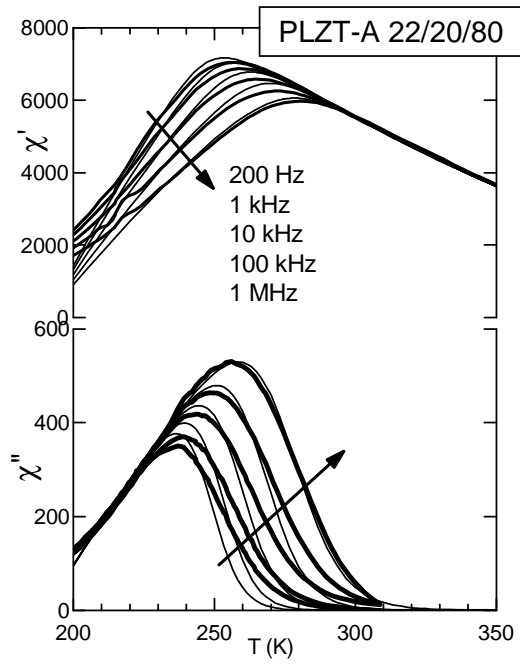


Fig. 5

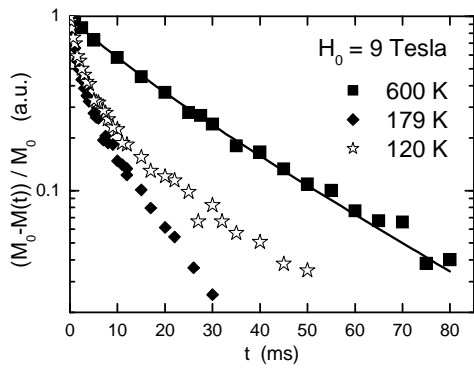


Fig. 6

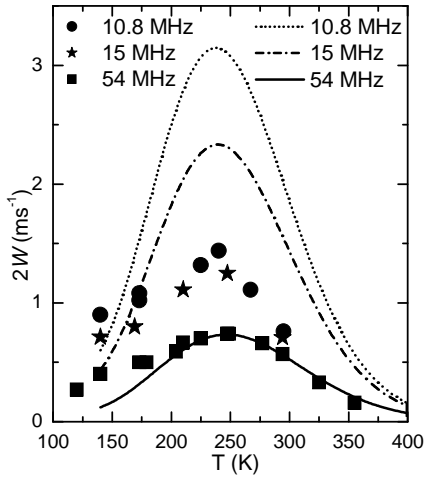


Fig. 7

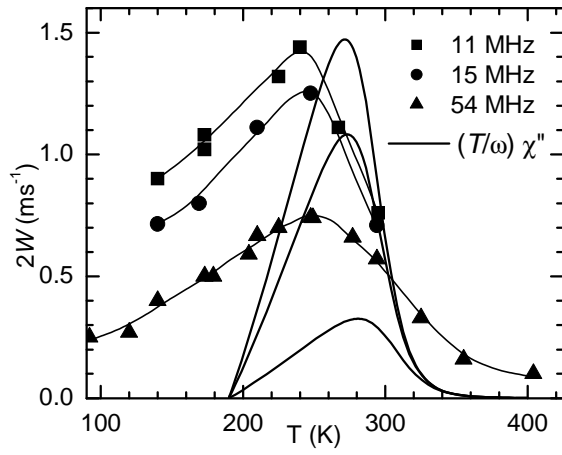


Fig. 8

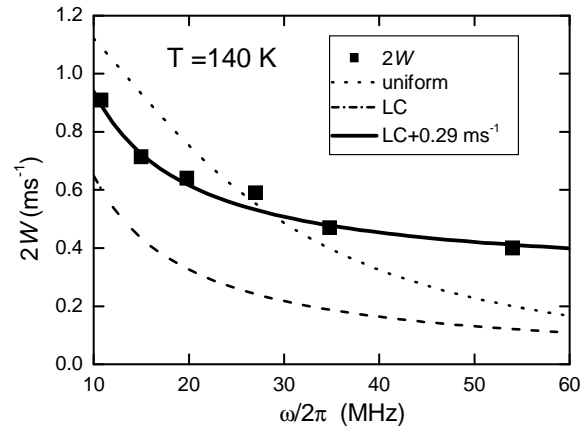


Fig. 9

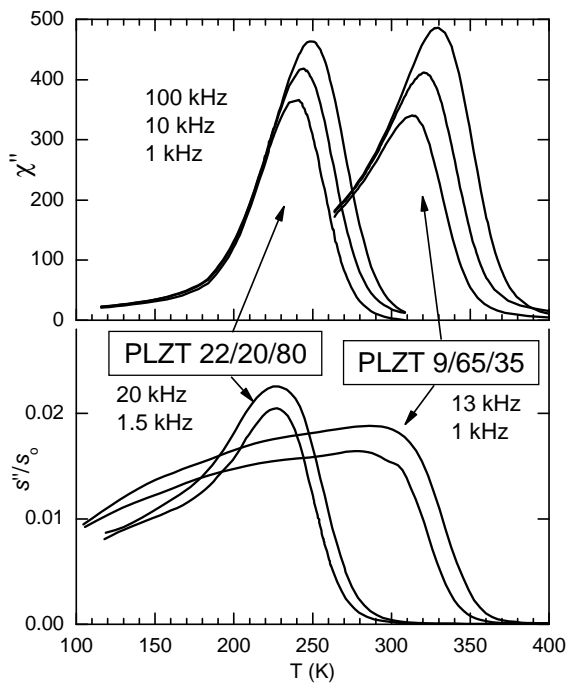


Fig. 10